S-/X-Band Microwave Optics Design and Analysis for DSN 34-Meter-Diameter Antenna

D. L. Nixon and D. A. Bathker
Radio Frequency and Microwave Subsystems Section

This article discusses the feed system configuration, RF optics design and predicted gain and noise temperature performance of the DSN 26 meter antenna S-/X-Band upgrade project. A previously developed and demonstrated dual band feed system employing separately located feeds, combined in a reflex-dichroic reflector arrangement, has been adapted to a particularly compact overall design. Special design techniques to minimize aperture blockage and then evaluate resultant performance are discussed in detail. Final predicted antenna gain and noise temperature performance values are given.

I. Introduction

A DSN 26-m antenna S-X Conversion Project has been undertaken to extend the capability of an existing 26-m subnet. This is being done to support typical long-lived outer planet missions and to offload the heavily scheduled 64-m network during mission cruise phases. The 26-m meter S/X Conversion Project has been described from an overall project view in Ref. 1. This report will cover the RF optics design and performance estimates. The modifications to the basic antenna system primarily include increasing the aperture diameter from 26 to 34-m and adding a simultaneous X-band capability. To achieve the X-band system, it was decided to continue use of the DSN reflex-dichroic feed (Ref. 2) very similar to that being used by the 64-m subnet. In the 34-m case, a single new Cassegrain feedcone housing large enough to enclose both the S-band and X-band feed systems was designed. In order to minimize aperture blockage, the feedhorn focal point location was substantially moved toward the paraboloid vertex and necessarily offset from the paraboloid axis. As a result of this, a new subreflector and quadripod are required, and are a part of the conversion.

This article will emphasize the microwave optics design considerations and the series of very detailed computations needed to predict overall microwave gain. Final computed estimates of overall antenna system gain and noise temperature at both S- and X-bands are given. Conclusions and recommendations to the project are included.

II. Feed System Configuration

Figure 1 shows the outline configuration of the 34-m upgraded antenna. The original 26-m-diam paraboloid focal length of 1097.28 cm (432.000 in.) is maintained; new outer panels according to the required contour are added. The initial 26-m system f/d ratio of 0.4235 is therefore substantially reduced to a new value of 0.3227; in effect a much "deeper" dish is formed. In order to minimize central blockage caused by the substantial size of the single large feedcone and associated reflex-dichroic reflectors,[1] the original 26-m-diam Cas-

[1]A description of the layout of the interior of the 34-m system feedcone is available in Ref. 3.

segrain design value for the separation of primary and secondary focal points of 579.12 cm (228.000 in.) is significantly increased to 701.04 cm (276.000 in.). This results in a feedhorn position above the paraboloid vertex fully 121.92 (48.000 in.) lower than the previous 26-m designs.

In the previous design, the feedhorn was visible, over the rim of the paraboloid, to an observer at a right angle to the antenna system boresight axis. In this new design, by a combination of the deeper dish and the increase in focal point separation distance, all feed components including the large ellipsoidal reflector are now within the envelope of the rim of the dish, as seen in Fig. 1. Also seen in this figure are the new quadripod feed support members, the necessarily larger apex structure, and the asymmetric subreflector. In contrast to the fully implemented 64-m system, wherein the asymmetric subreflector is rotatable about the paraboloid axis (to obtain switching among the three separate feedcones used in that system), the 34-m design described here uses a fixed subreflector, permanently focussed upon the X-band feedhorn focal point, located below the dichroic plate.

A cross-sectional detailed view of the reflex feed system geometry is shown in Fig. 2. Four of the elements, the S- and X-band feedhorns, the ellipsoidal reflector and the planar dichroic reflector as well as the critical relative positions of these four elements, are borrowed directly from the previously demonstrated 64-m design (Refs. 2 and 4). With these critical relative positions held constant, the optics design proceeded by rocking the subassembly about the primary focal point at the radius value equal to 701.04 cm (276.000 in.), until an approximately equal central blockage condition was achieved. This occurred, as shown in both Figs. 1 and 2, with an offset angle of 7.6677 deg. This offset angle, once determined, then allows design of the subreflector to proceed.

The subreflector consists of three parts; the hyperboloidal surface contour, the non-optic peripheral flange, and the non-optic vertex plate. The peripheral flange was iteratively designed by use of computed scattered patterns, noting the decrease in power spilled past the rim of the paraboloid, at both S- and X-bands. This is a key parameter in determining the noise performance of the finished design. The vertex plate was added to decrease the RF illumination into the central zone containing the feedcone and reflex reflectors.

III. Blockage

A rather novel approach in determining the blockage was used for this project. A precision scale shadow drawing (Fig. 3) was generated by using a computer. As can be seen, this includes direct optical planewave blockage as well as spherical wave shadows caused by any structure in the RF paths. The hyperboloid outline, the apex portion of the quadripod, and the inner part of the quadripod shadows were projected on the planewave basis. All other shadows were projected from the paraboloidal focal point, on a spherical wave basis. The total blockage was then determined by mechanically integrating the complex outline to get the shadow area for all structures and comparing that to the overall paraboloid projected area. This results in a total of 4.24% for quadripod blockage and 1.82% central area blockage giving a total of 6.06% area blockage. It should be noted that this is the physical (optical) blockage; very short wavelength RF blockage will be essentially equal while longer wavelengths will typically be affected somewhat more than the optical value. At both S- and X-bands we estimate the true value to be close to the optical value.

IV. Vertex Plate

As mentioned, a vertex plate for the subreflector is considered an especially important part of the overall RF optics design for the 34-m S/X system. In many systems, vertex plates are employed totally or primarily to reduce the hyperboloid axial backscatter into the feedhorn, which results in feed system VSWR which, in turn, alternates with small changes in operating frequency because of the long (in wavelengths) path involved. As the size of a given Cassegrain system increases relative to wavelength, the behavior is such that the VSWR decreases. For a perfectly axial system of the 34-m S/X size, the estimated hyperboloid VSWR is 1.08:1 at S-band and substantially less at X-band. One concludes from this that a vertex plate for the 34-m S/X system is desirable at S-band, but not particularly useful at X-band, from a VSWR viewpoint. In this design, the large central blockage area (1.82%) caused by the substantial shadows from the feed system reflectors (ellipsoid-dichroic), leads one to question the amount of power contained within that area, assuming both feeds in transmission.[2] The amounts of power in the subject area were obtained from scattered patterns (without vertex plate) as 4.7 and 4.0% at S- and X-bands, respectively. If uncontrolled, this power would be scattered into generally unpredictable wide-angle pattern regions, by way of radiation off of the backside of the ellipsoidal reflector, feedcone sides, etc. One concludes from this that a vertex plate for the 34-m S/X system is highly desirable at both frequency bands.

A vertex plate was designed on an iterative basis using primarily the scattering program (FVSCATT) and the radiation pattern efficiency program (EFFIC). Also, other programs

[2]Reciprocity can alternately be considered to show the feeds in reception will be sensitive, at that power percentage, to whatever radiation (noise, perhaps) might emanate from that area (via reflections, for example).

used were (CASSDESIGN), (AZEXP), and (ANTPLOT).[3] Vertex plates tend to be narrowband devices (in the sense of a frequency span from S- to X-bands), by virtue of the principle of displaced phase centers (displaced from the hyperboloid center of radiation). Nonetheless, a design was obtained and evaluated, resulting in the following performance. At S-band, the 4.7% central blockage zone power was reduced to 1.7%. The corresponding central blockage efficiency factor, (a function of blocked area and power) increased from 0.9197 to 0.9651. At X-band, the 4.0% central blockage zone power was reduced to 0.5%. The corresponding central blockage efficiency increased from 0.9430 to 0.9771.

On an overall efficiency basis, however, the above increases in the central blockage efficiency term are not necessarily realized as a final benefit. This is because the aperture illumination phase efficiency is typically degraded somewhat by including a vertex plate in a given design. In the 34-m S/X design discussed here, the phase efficiency degradations incurred as a result of using a vertex plate are 0.9 and 4.5% at S- and X-bands respectively. Other factors such as aperture illumination amplitude efficiency are impacted in minor ways; the overall efficiency at S-band was improved 0.14 dB by use of the vertex plate while the X-band was degraded 0.18 dB. In view of the overall operating system gain to noise temperature ratio, the tradeoff of 0.18 dB of X-band gain for the benefits of controlling most of the 4% stray radiation at X-band is considered highly desirable.

V. Azimuthal Mode Analysis

As seen in Figs. 1 and 2, the 34-m design includes the large offset feed angle of 7.7 deg as a key unavoidable feature of the design. This is a necessarily large angle due to the relatively shorter focal length of the 34-m antenna. One result of the large offset feed angle inherent in this size antenna is that the subreflector is substantially more asymmetric than in our previous 64-m designs. For example, the 64-m offset feed angle is approximately 4.5 deg; a gain degradation of 0.009 dB results from $m \neq 1$ mode conversion due to this amount of asymmetry (Ref. 4). One of the major design complexities of the 34-m RF optics design was to understand the impact of the expected additional mode conversion and associated gain degradation. As will be shown in the section on computed antenna gain, the gain degradation increased to 0.042 dB due to the greater relative asymmetry of the 34-m subreflector.

The azimuthal analysis of feed radiation patterns is well documented in previous literature (Refs. 2, 5, 6, 7), showing that only $m = 1$ components of the pattern contribute to the antenna gain. Energy contained in the $m \neq 1$ components represents a degradation of antenna gain and, in a receive mode, a possible source of system noise temperature degradation.

A computer program (AZEXP) was used to individually compute the azimuthal mode component patterns. The input to this program is a group of radiation patterns obtained from the (FVSCATT) program. The computed output from (AZEXP) is a series of polar patterns for each m index from 0 to 3, together with the total power in each of the m-component patterns. The resulting modal power for S- and X-band as scattered from the subreflector is presented in Fig. 4. As can be seen in Fig. 4 there is significant power in the $m \neq 1$ modes. Not all of the reductions seen in the $m \neq 1$ terms in Fig. 4 result in overall antenna gain loss, however. Figure 4 addresses the relative amounts of mode power while the previously mentioned gain degradation of 0.042 dB (at X-band), which will be discussed further in Table 2, is representative of that portion that is destructive to the desired polarization. When using circular polarization, there is enough energy in these $m \neq 1$ modes to cause shift of the secondary beams of the overall antenna system. A preliminary analysis of this beam shift indicates a 0.004-deg shift at X-band and a 0.04-deg shift at S-band. (The corresponding gain loss at S-band, assuming perfect pointing is achieved at X-band, is 0.34 dB).

VI. Total System Noise Temperature

The total system noise temperature as a function of elevation angle is expected to be very similar to the 64-m antennas. The values shown in Fig. 5 are estimates of what to expect from the new 34-m design. The tolerance is ±3.0 K for X-band and ±2.5 K for S-band. The graphs do not extend below 20 deg elevation because of the difficulty of accurate prediction at such low angles. Final performance values will be determined from field measurements.

VII. Computed Performance

The design and evaluation of the 34-m S/X upgrade involved many computer programs. The major programs are listed in Table 1.

A brief narrative of the computational process is as follows, starting with the S-band system. A standard JPL corrugated conical feedhorn (Ref. 8) is used. First, the horn E- and H-plane amplitude and phase data from radiation patterns shown in Fig. 6 are numerically scattered off the ellipsoidal reflector using the computer program (FSCAT). The output from this program is shown in Fig. 7 and is then scattered off of the dichroic flat plate, using (FSCATT) a second time. That

[3] A summary of these and other JPL programs used is given in Table 1.

output, shown in Fig. 8 is then scattered off of the subreflector including a vertex plate and flange using (FVSCATT). This final output shown in Fig. 9 can then be evaluated using (AZEXP) and (EFFIC) to determine the overall illumination efficiency of the main paraboloid. It should be noted that a complex set of antenna patterns are used throughout this process with m modes of $m = 0$, $m = 1$, $m = 2$, and $m = 3$ included. This preserves and sums the beam asymmetry accumulation as it develops from each surface.

The X-band system evaluation is much simpler, because no asymmetric ellipsoid is present; of course, the asymmetric subreflector introduces the need for azimuthal modal decomposition analysis. The feedhorn radiation patterns (Fig. 6) (the S- and X-band feedhorn are the same design simply scaled for frequency) were scattered off of the same subreflector as the S-band system using (FVSCATT). The resultant illumination patterns are shown in (Fig. 10). This was the final scattering output and was evaluated using (AZEXP) and (EFFIC) similar to the S-band process.

VIII. Calculated Antenna Gain

Using the antenna patterns that were generated as described earlier, and at each stage preserving the azimuthal modes $m = 0$, 1, 2 and 3, the various antenna efficiency components are computed as shown in Table 2.

The predicted paraboloid/subreflector surface tolerance ranges from a low of 0.58 mm at reasonable elevation angles with no wind or thermals to a maximum of 1.0 mm at 60 deg elevation with wind and thermal distortion included. This maximum gives a gain loss at X-band of 0.51 dB and at S-band 0.04 dB. The higher RMS of 1.0 mm was used for the antenna gain in Table 2.

The gain values are defined at the input to the maser preamplifiers. The S-band gain as indicated in Table 2 is for the S-band low noise system. The expected gain for the S-band diplex mode is 0.09 dB less. The expected tolerance for X-band is +0.3 dB to −0.9 dB and the S-band gain tolerance is ±0.6 dB. These tolerances include the major error sources which will be incurred during field measurements using natural radio sources. As stated in the section on azimuthal mode analysis, beam squint at S-band, due to higher order mode generation as a result of the asymmetric design, will degrade the S-band gain by 0.34 dB below the peak value indicated in Table 2. Thus, the operational system, assuming X-band beam peak pointing, is predicted to operate with +67.0 dB X-band gain and +56.1 dB S-band gain (low noise path) or +56.0 dB (diplex path).

IX. Summary and Recommendations

This report discusses the feed system configuration selected for the DSN 34-m S/X project (26-m antenna upgrade). A previously developed and demonstrated dual-band feed system employing separately located conventional feeds, combined in a reflex-dichroic reflector arrangement, has been adapted to a particularly compact overall design. It is an inescapable characteristic of this design that moderate to high central aperture blockage exists, as well as a higher degree of offset feed asymmetry than before. For these reasons, special analyses were done emphasizing blockage minimization and evaluation, including vertex plate design, as well as azimuthal mode analysis of the resultant moded illumination patterns on the paraboloid surface. Secondary beam squint was obtained at both frequency bands. Nevertheless, quite acceptable overall antenna gain and noise temperature performance at both frequency bands is indicated.

It is recommended that the project budget sufficient radio frequency (RF) system performance test time, following initial installation, and plan for a full evaluation of RF system parameters, especially overall system noise temperature at low elevation angles. Because the CONSCAN secondary beam pointing scheme as well as the subreflector focusing as a function of HA-Dec angles are very important to the RF performance achievement goals of the project, sufficient additional test time for a complete evaluation of those parameters is necessary. Finally, secondary beam squint between the two frequency bands requires evaluation in the field.

References

1. Lobb, V. B. , "26 Meter S-X Conversion Project," *The Deep Space Network Progress Report No. 39,* Jet Propulsion Laboratory, Pasadena, Calif., June 15, 1977.

2. Potter, P. D., "S- and X-Band Feed System," Technical Report 32-1526, Vol. VIII, pp. 53-60, Jet Propulsion Laboratory, Pasadena, Calif., April 15, 1972.

3. Hartop, R. W., "Dual Frequency Feed System for 26-Meter Antenna Conversion," *DSN Progress Report 42-40,* pp. 146-149. Jet Propulsion Laboratory, Pasadena, Calif., Aug. 15, 1977.

4. Bathker, D. A., "Dual Frequency Dichroic Feed Performance," presented at the XXVI Meeting of the Arronus Panel, NATO-AGARD, Munich, Germany, Nov. 26-30, 1973.

5. Ludwig, A. C., "Calculation of Scattered Patterns from Asymmetrical Reflectors," Technical Report 32-1430, Jet Propulsion Laboratory, Pasadena, Calif., Feb. 15, 1970.

6. Potter, P. D., "Application of Spherical Wave Theory to Cassegrainian-Fed Paraboloids," *IEEE Trans. Ant. Prop.,* Vol. AP-15, No. 6, pp. 727-736, November 1967.

7. Ludwig, A. C., "Near-Field Far-Field Transformations Using Spherical-Wave Expansions," *IEEE Trans. Ant. Prop.,* Vol. AP-19, No. 2, pp. 214-220.

8. Brunstein, S. A., "A New Wideband Feedhorn with Equal E- and H-Plane Beamwidths and Suppressed Sidelobes," *Space Programs Summary 37-58,* Vol. II, pp. 61-64, Jet Propulsion Laboratory, Pasadena, Calif., July 1969.

9. Ludwig, A., "Antenna Feed Efficiency," *Space Programs Summary No. 37-26,* Vol. IV, pp. 200-208, Jet Propulsion Laboratory, Pasadena, Calif., April 30, 1964.

10. Potter, P. D., *A Computer Program for Machine Design of Cassegrain Feed Systems,* Technical Report 32-1202, Jet Propulsion Laboratory, Pasadena, Calif., Dec. 15, 1967.

Table 1. Antenna design computer programs

Name	Use
SPWEXP	Spherical wave expansion and fields calculation (Ref. 7)
FSCATT	Asymmetrical scattering (Ref. 5) (general conic surface)
AZEXP	Antenna pattern aximuthal fourier analysis (Ref. 5, Appendix A)
ANTPLOT	Antenna pattern plotting
EFFIC	General case efficiency (Ref. 9)
ANTDESIGN	Offset feed geometry
CASSDESIGN	Cassegrain feed system design (Ref. 10)
FVSCATT	Asymmetrical scattering (hyperbolic subreflector with flange and vertex plate)
NEWGRID	Grid spacing for FVSCATT
FLATGRID	Flat grid for FSCATT (dichroic plate)
FLATSURF	Flat surface input to FSCATT (dichroic plate)
FSURFELP	Ellipsoidal surface for FSCATT
FSURFGRID	Ellipsoidal grid for FSCATT

Table 2. 34-m Reflex feed system gain — S- and X-bands

Efficiency Component	X-Band 8.415 GHz		S-Band 2.295 GHz	
	Ratio	dB	Ratio	dB
Forward spillover	0.96005	-0.1771	0.98231	-0.0775
Rear spillover	0.99568	-0.0188	0.99637	-0.0158
Non-uniform amplitude illumination	0.84289	-0.7423	0.83582	-0.7789
Non-uniform phase illumination	0.91297	-0.3954	0.96398	-0.1593
Cross polarization	0.99942	-0.0025	0.99975	-0.0011
Mode conversion ($m \neq 1$)	0.99038	-0.0420	0.97503	-0.1098
Central blockage	0.9771	-0.1006	0.9651	-0.1543
Quadripod blockage (optical)	0.9170	-0.376	0.9170	-0.376
Paraboloid/subreflector surface tolerance loss (1.0 mm RMS)	0.88209	-0.5448	0.99096	-0.0394
Ellipsoid reflector tolerance loss (0.51 mm RMS)	Not applicable		0.99759	-0.0105
Transmission loss through planar reflector	0.9950	-0.0218	Not applicable	
Waveguide dissipative loss	0.9757	-0.107	0.9772	-0.100
Overall efficiency	0.5587	-2.529	0.6572	-1.823
Gain for 100% efficiency	8.9893×10^6	69.537	6.68623×10^5	58.252
Overall gain		67.01		56.43

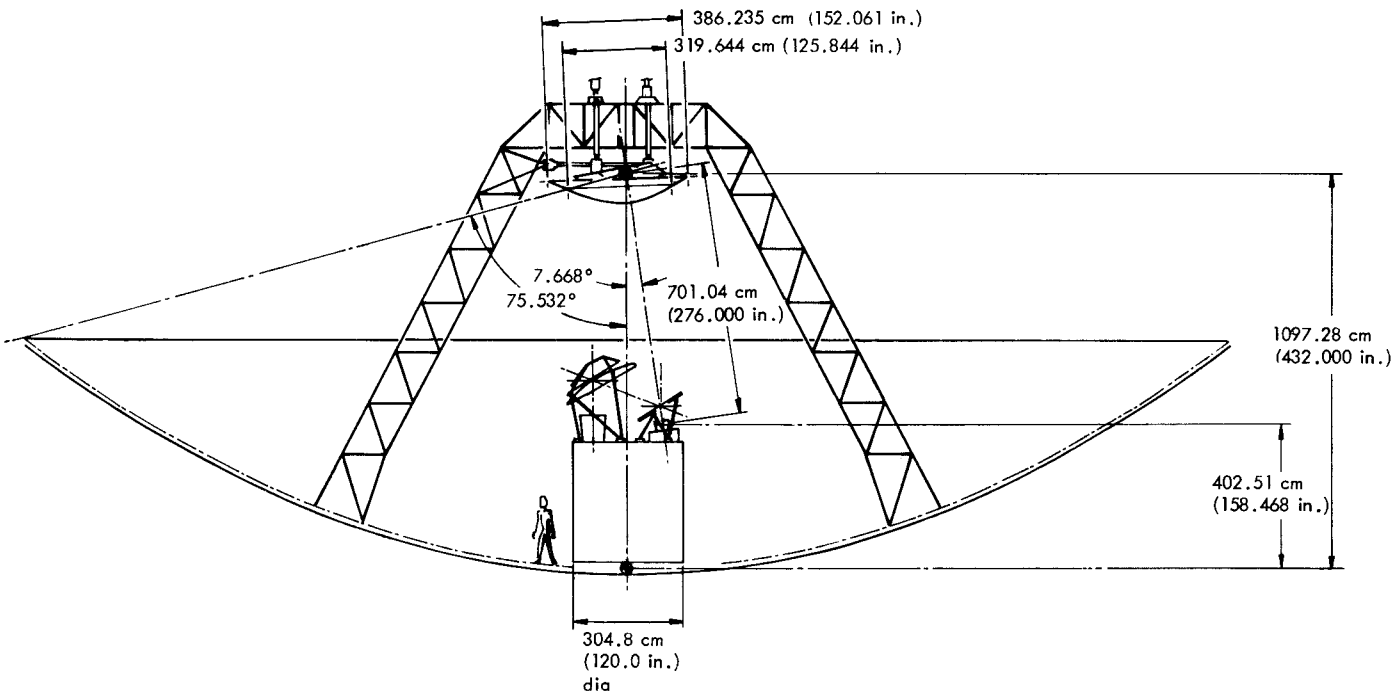

Fig. 1. 34-m S/X band antenna configuration

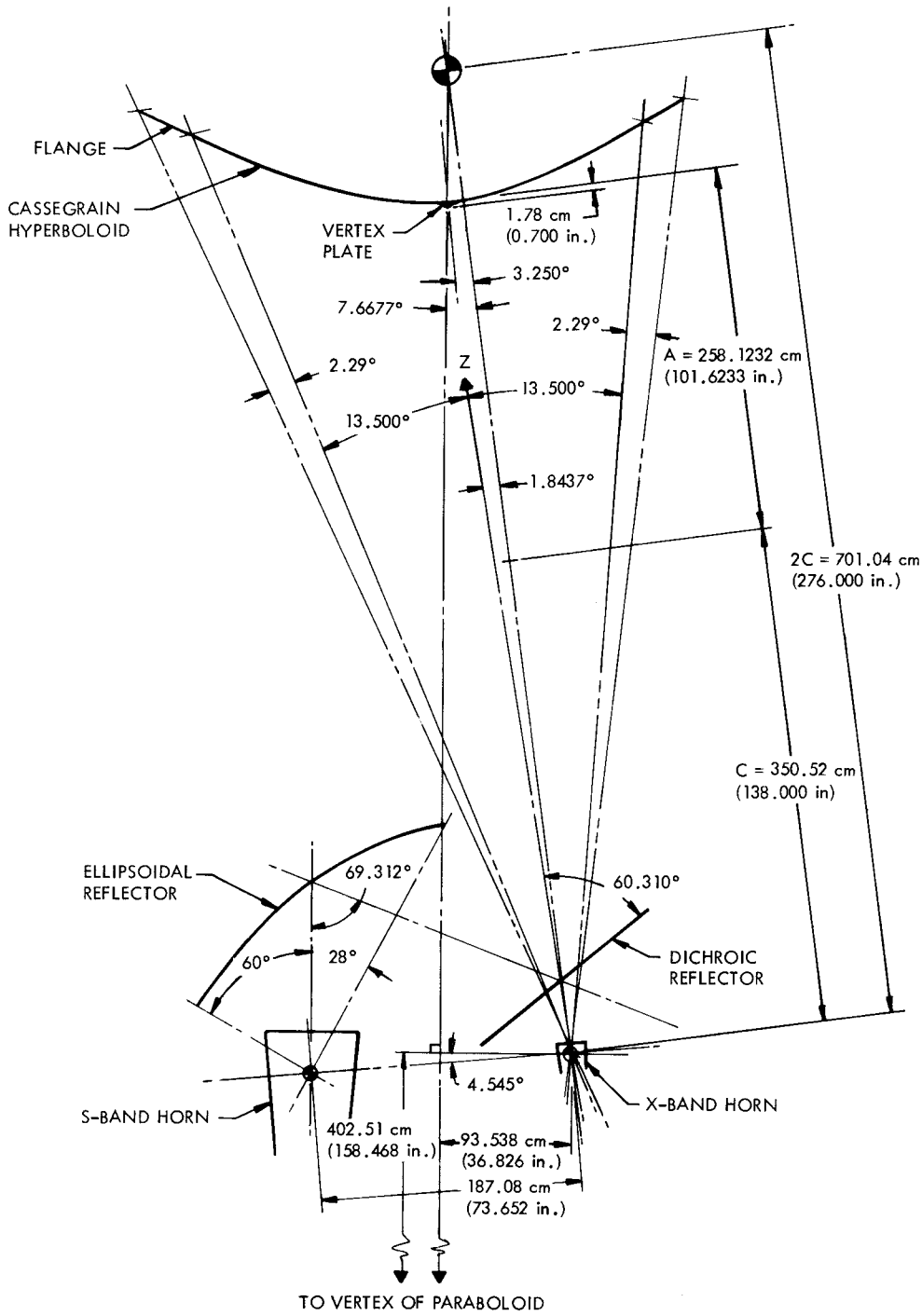

Fig. 2. 34-m S/X band reflex feed geometry

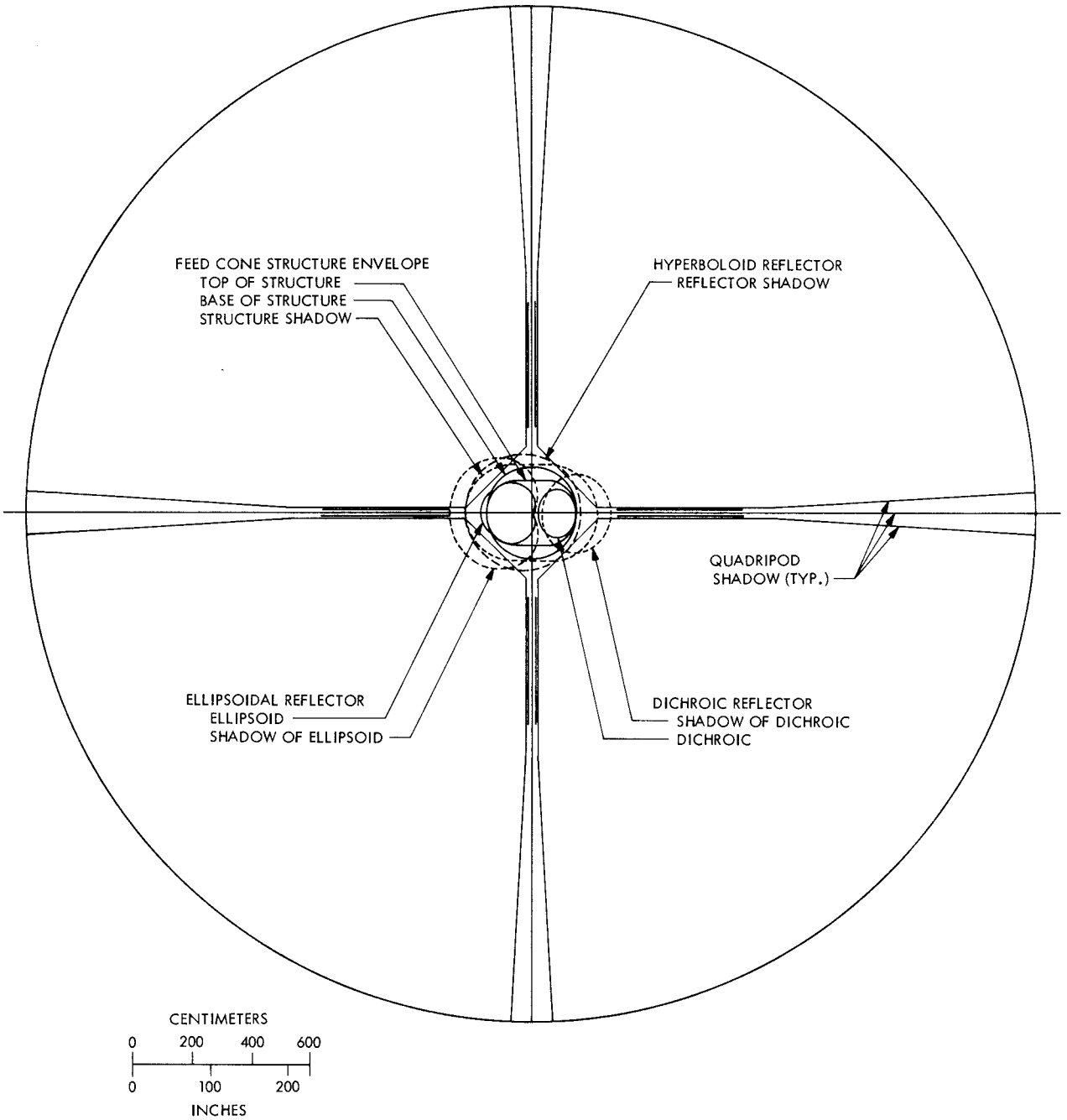

Fig. 3. Computed shadow drawing

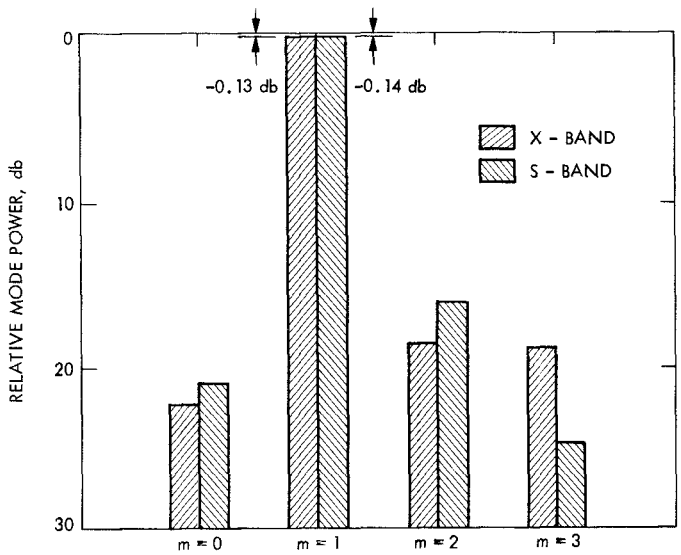

Fig. 4. Azimuthal mode power in the subreflector patterns, 34-m S/X system

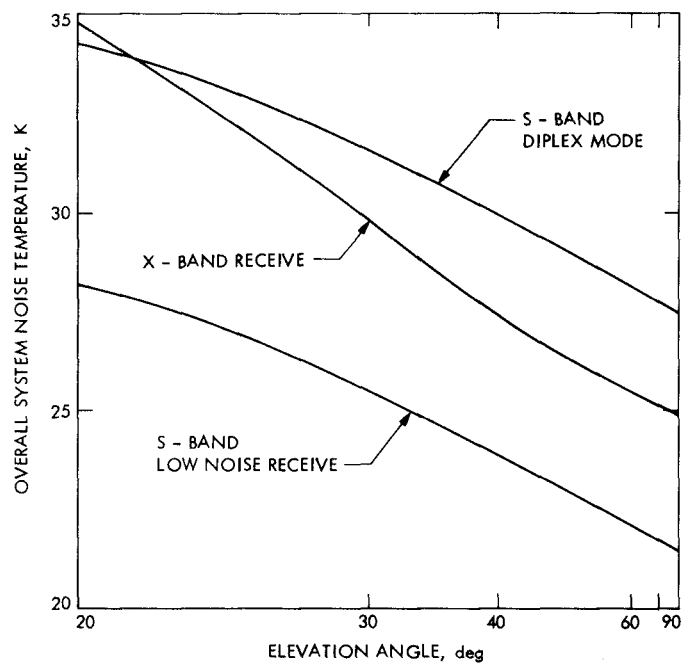

Fig. 5. 34-m S/X overall system noise temperature

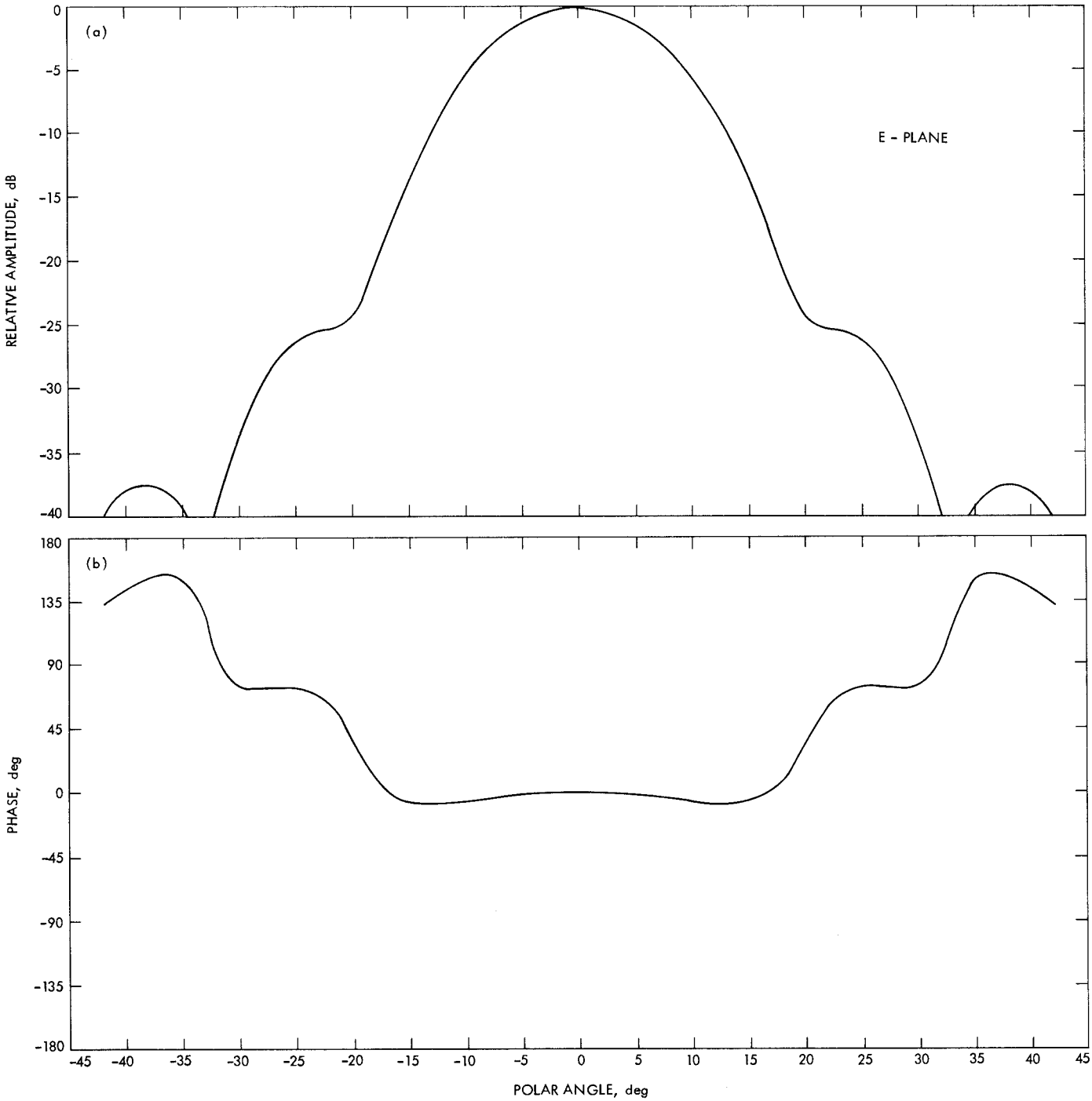

Fig. 6. S- and X-band 22-dB theoretical horn patterns: (a) E-plane amplitude and (b) E-plane phase

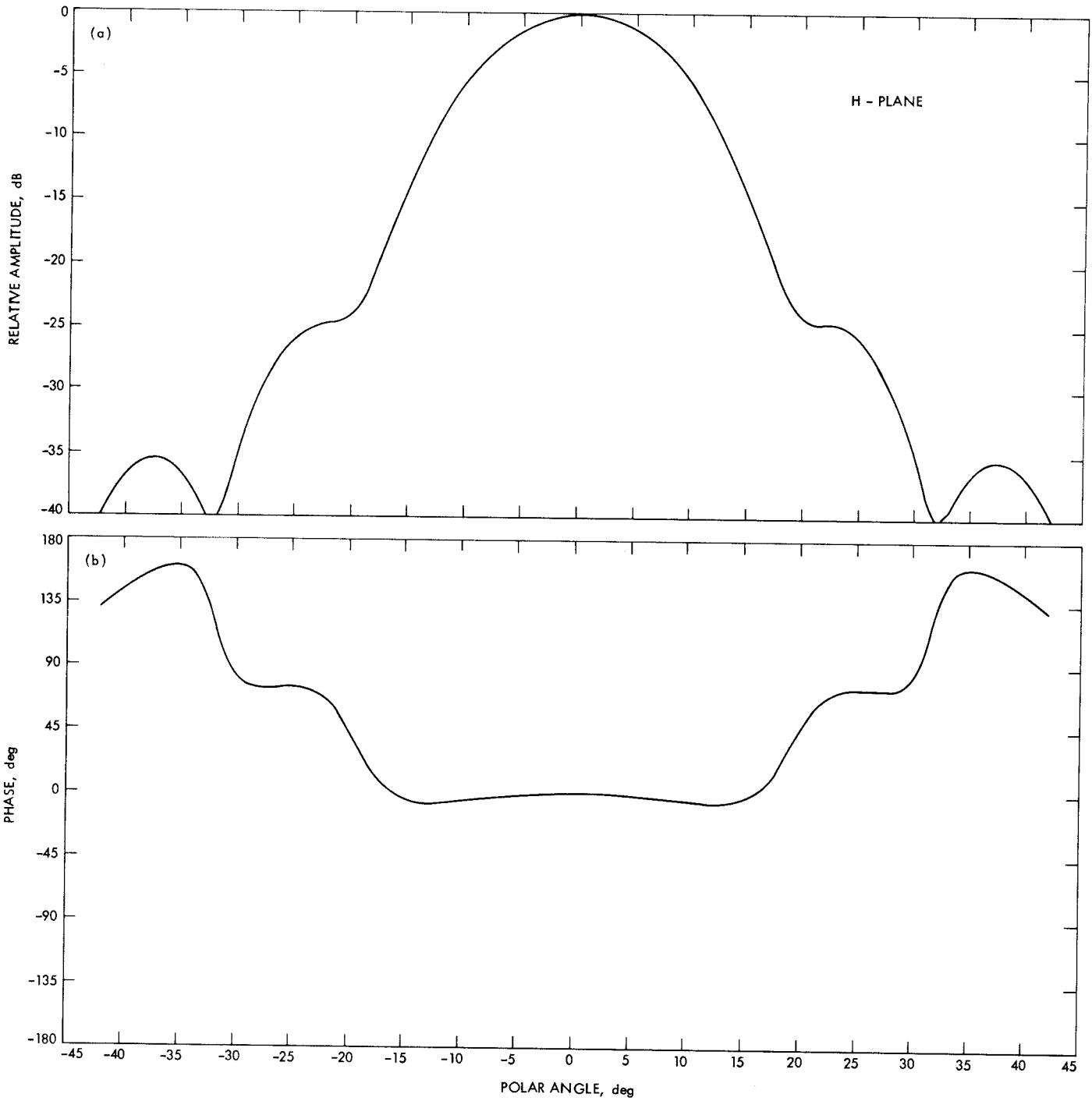

Fig. 7. S- and X-band 22 dB theoretical horn patterns: (a) H-plane amplitude and (b) H-plane phase

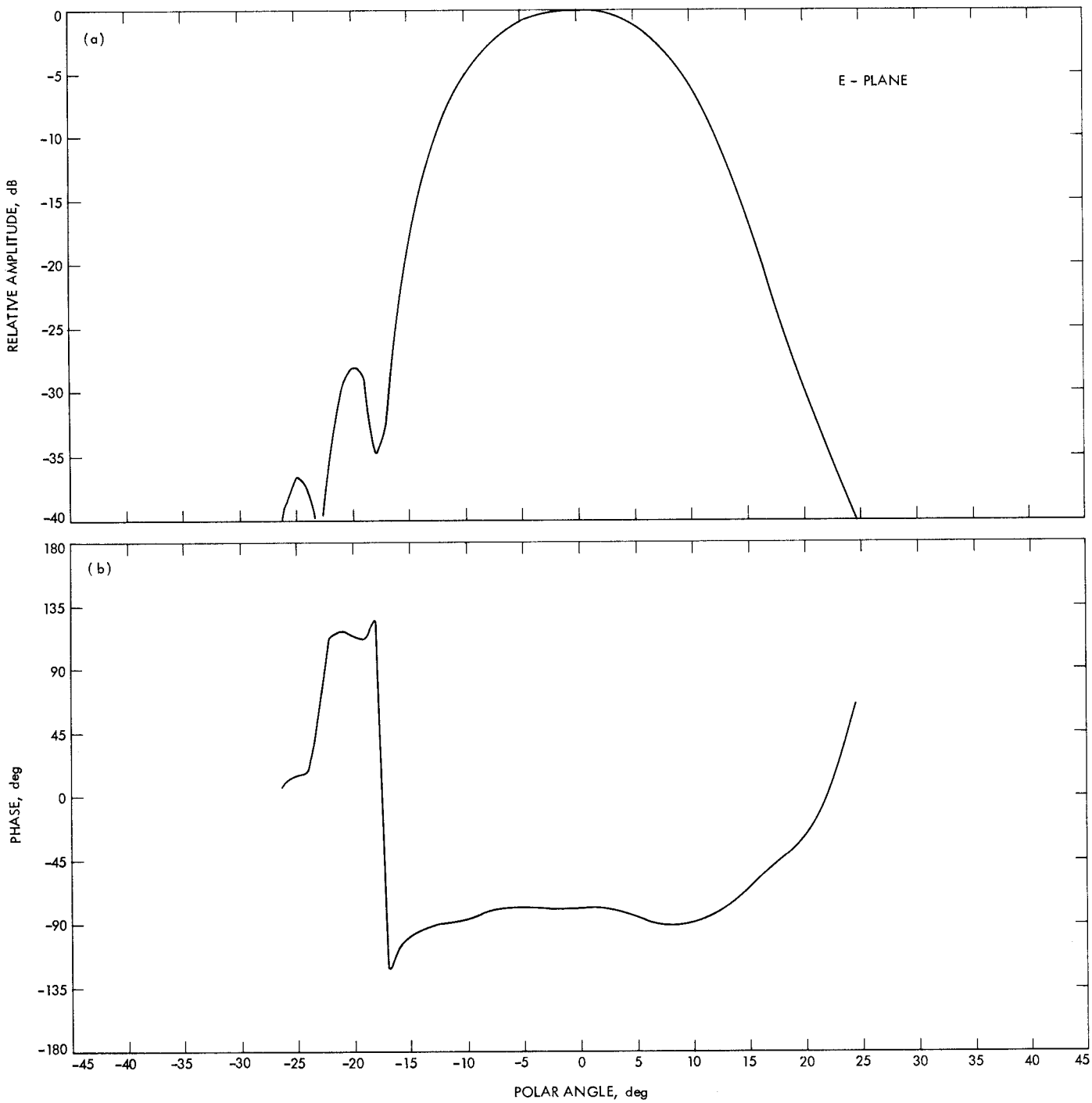

Fig. 8. S-band 34/64-m system: ellipsoid and dichroic plate (a) E-plane amplitude and (b) E-plane phase

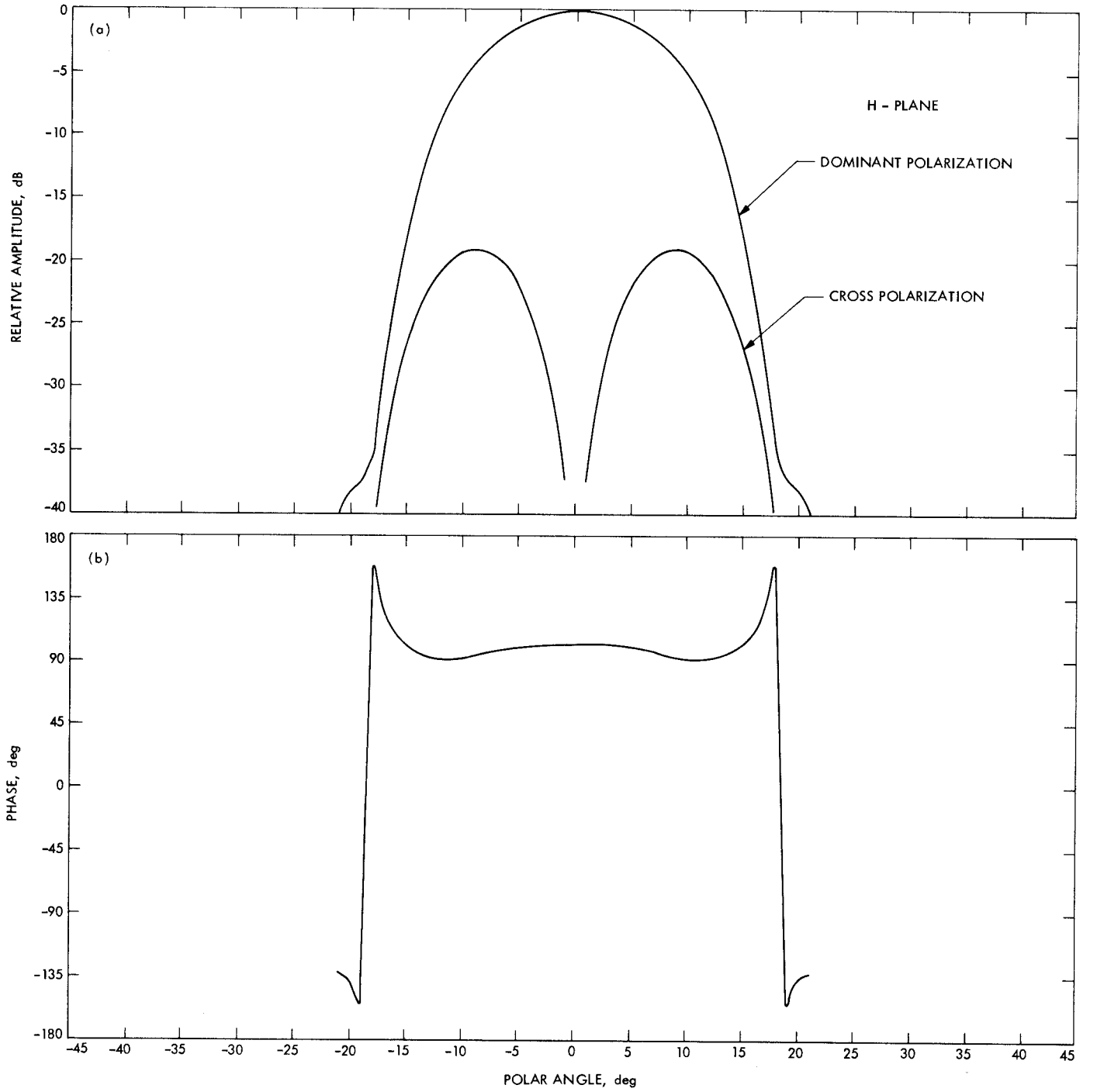

Fig. 9. S-band 34/64-m system: ellipsoid (a) H-plane amplitude and (b) H-plane phase

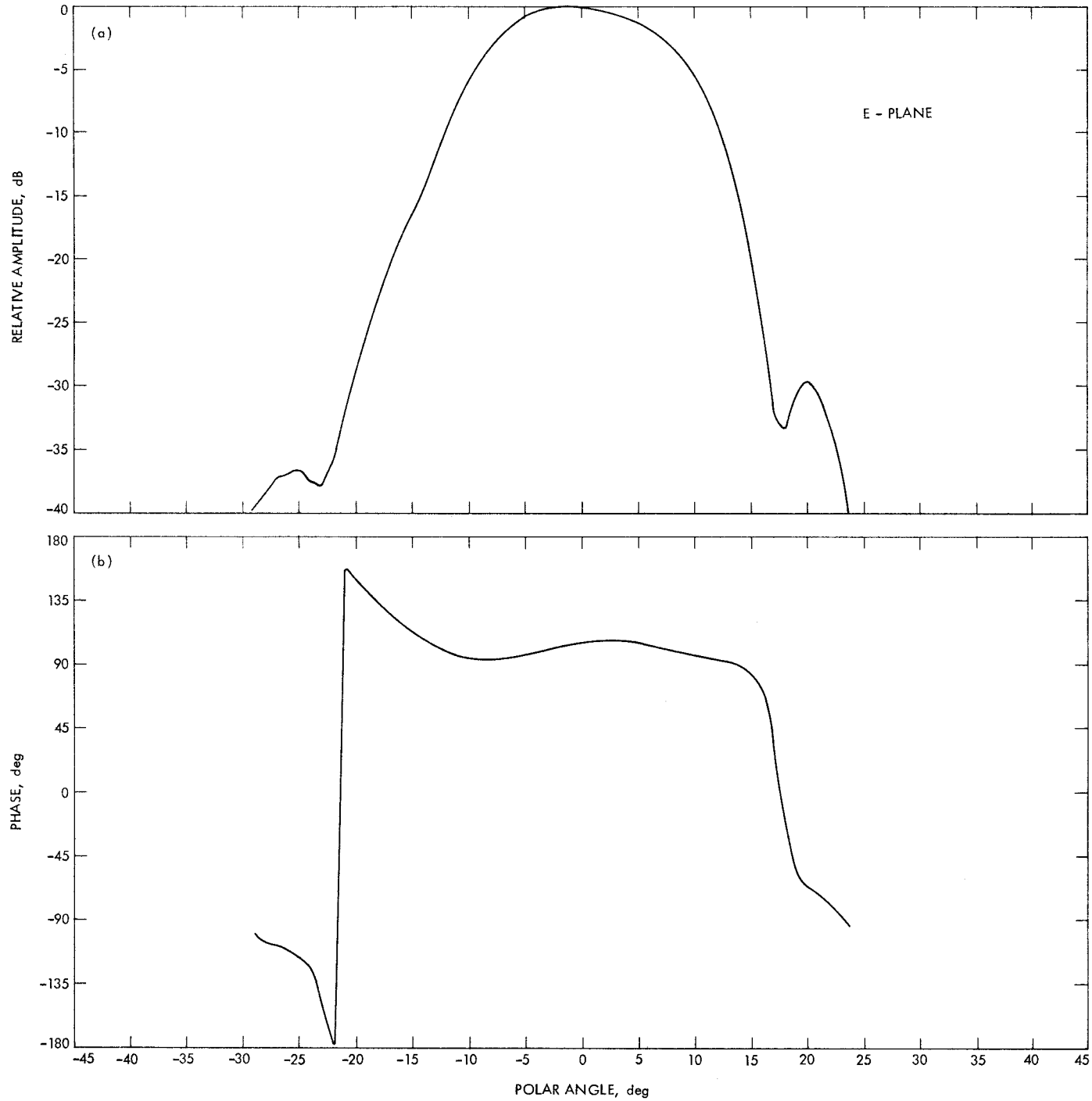

Fig. 10. S-band 34/64-m system: ellipsoid and dichroic plate (a) E-plane amplitude and (b) E-plane phase

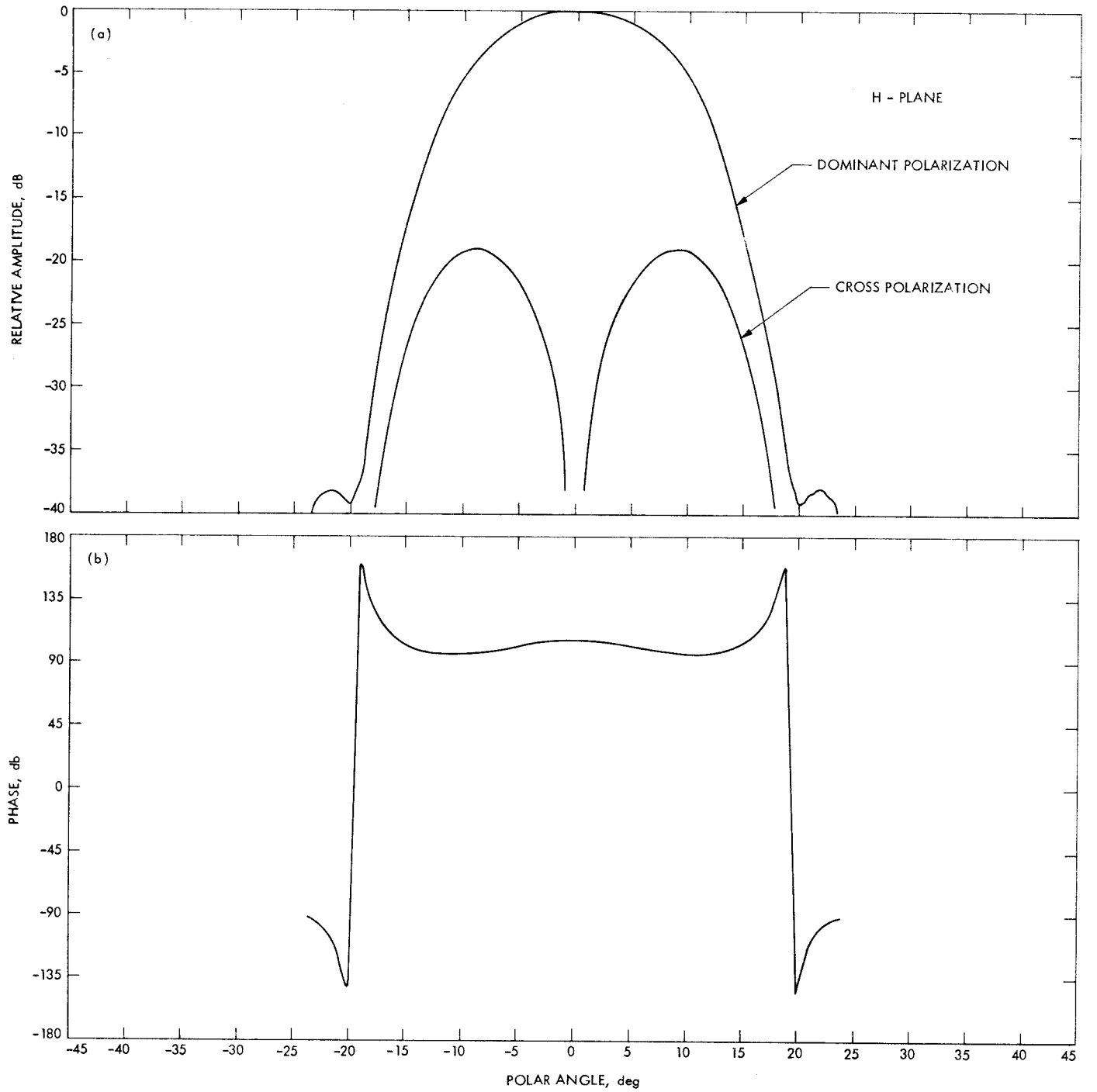

Fig. 11. S-band 34/64-m system: ellipsoid and dichroic plate (a) H-plane amplitude and (b) H-plane phase

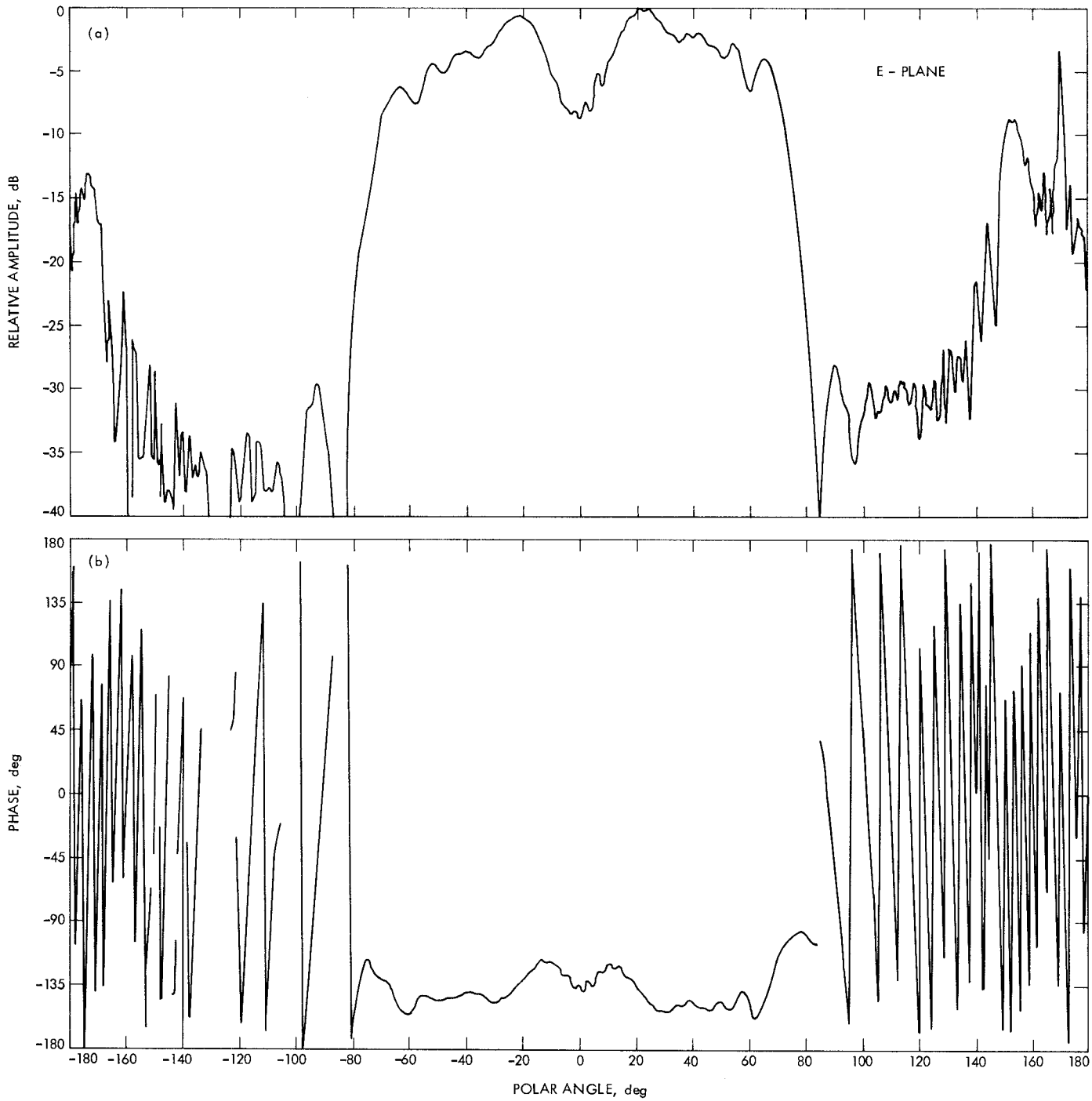

Fig. 12. S-band 34-m system: ellipsoid, dichroic plate, and subreflector (a) E-plane amplitude and (b) E-plane phase

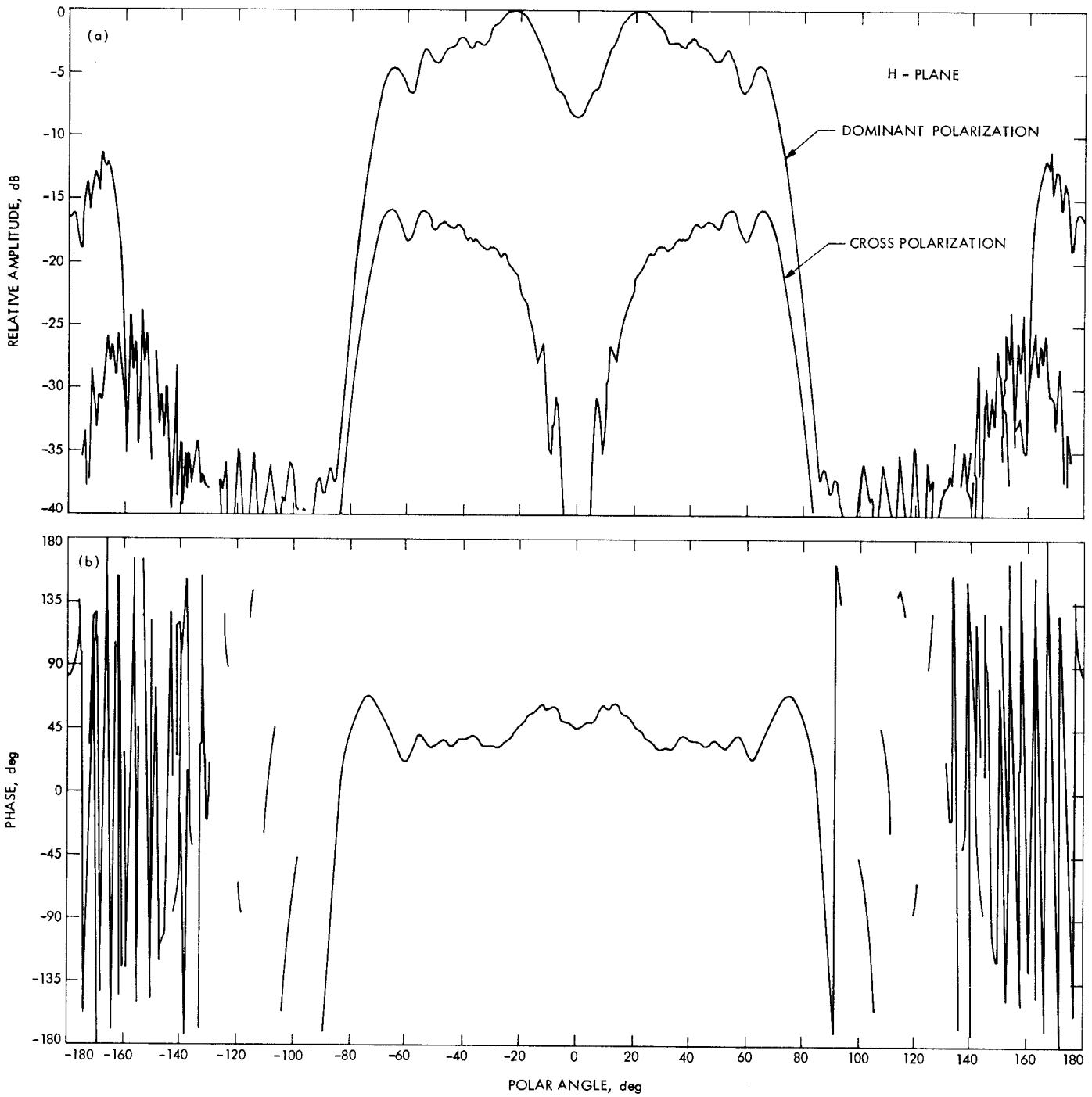

Fig. 13. S-band 34-m system: ellipsoid, dichroic plate, and subreflector (a) H-plane amplitude and (b) H-plane phase

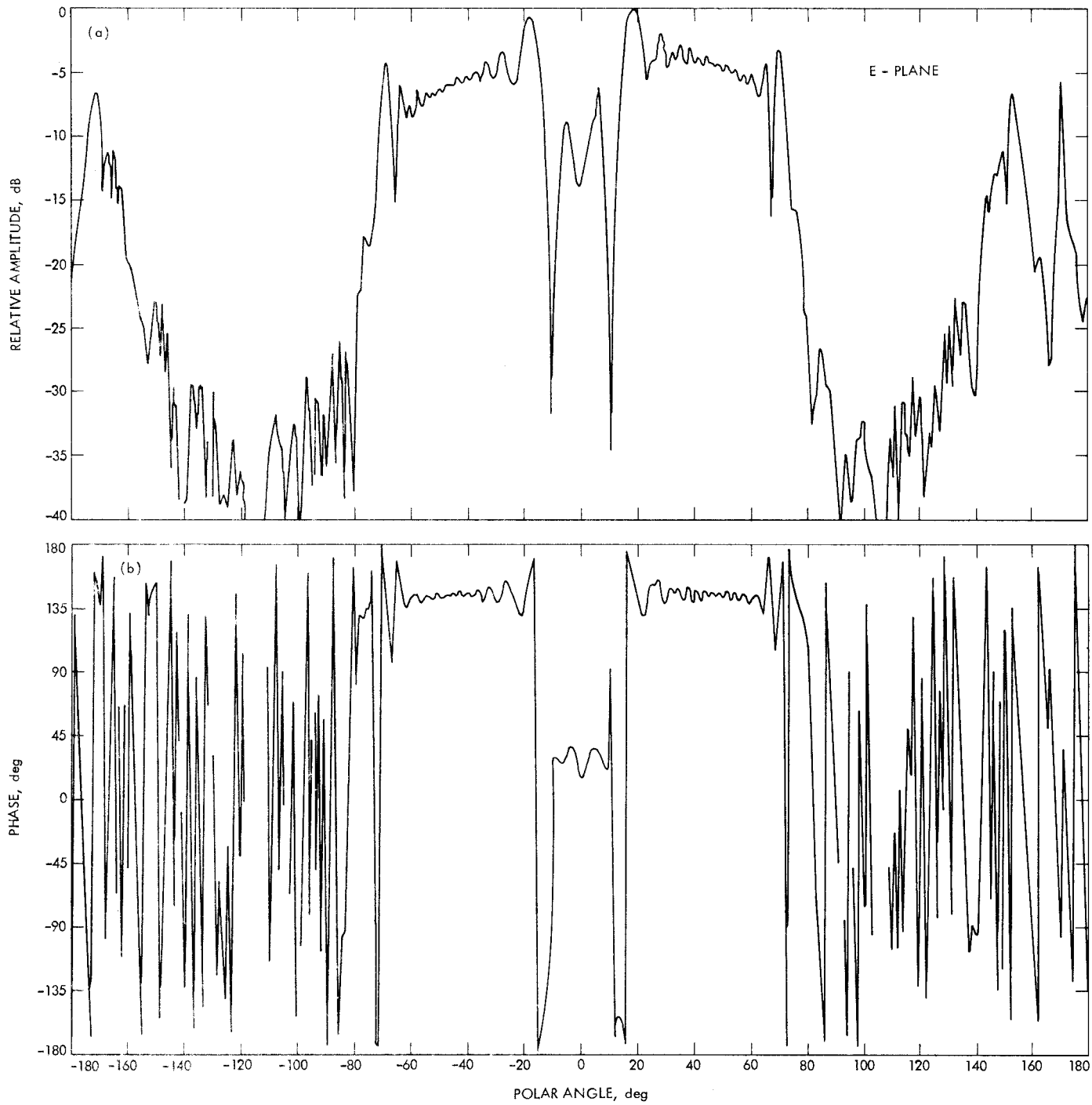

Fig. 14. X-band 34-m system: subreflector (a) E-plane amplitude and (b) E-plane phase

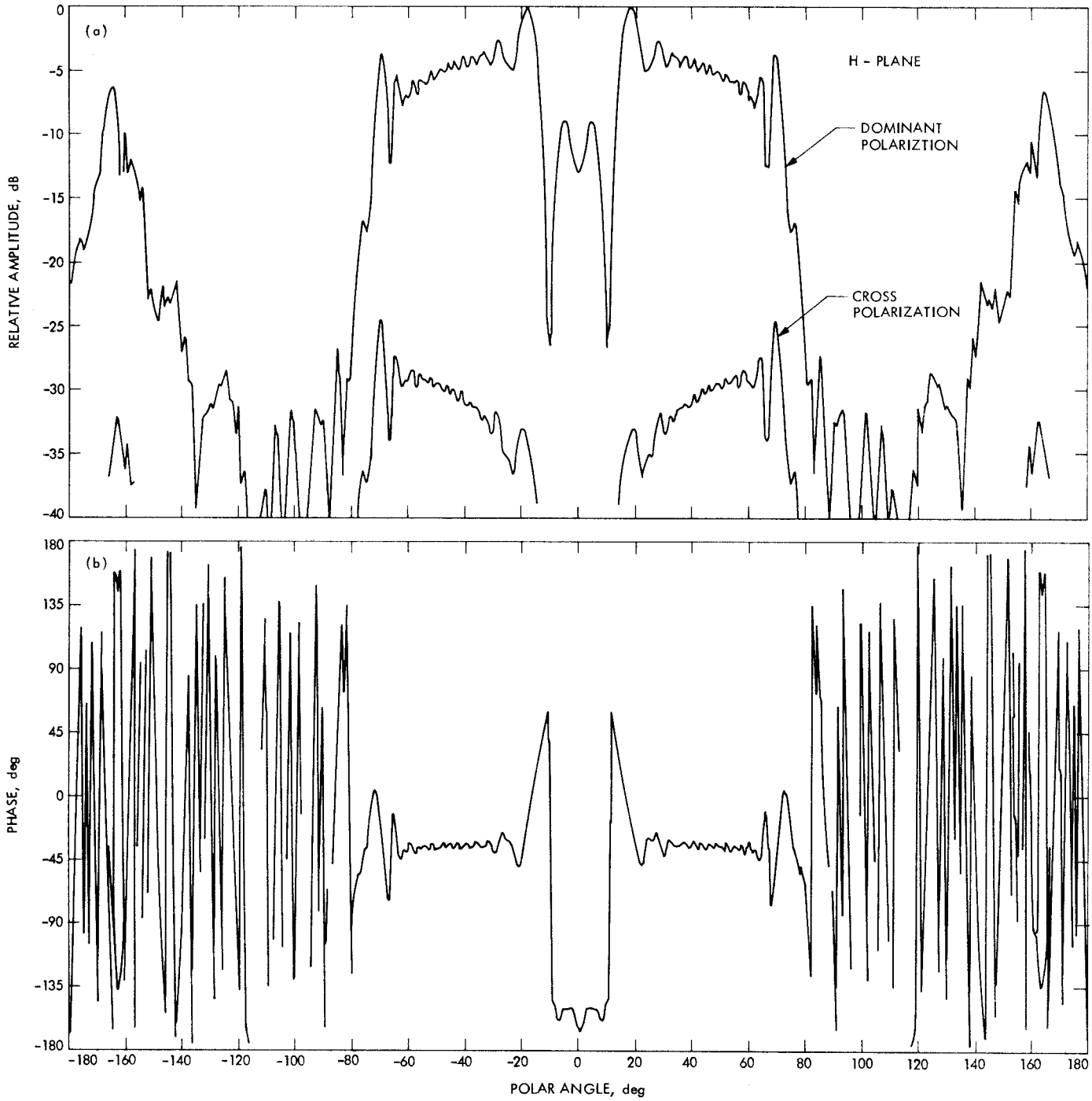

Fig. 15. X-band 34-m system: subreflector (a) H-plane amplitude and (b) H-plane phase